Experimental Eye Research xxx (2010) 1–9

Contents lists available at ScienceDirect

Experimental Eye Research

journal homepage: www.elsevier.com/locate/yexer

Finite element modeling of the human sclera: Influence on optic nerve head biomechanics and connections with glaucoma

Richard E. Norman [a,b], John G. Flanagan [c,d], Ian A. Sigal [e], Sophie M.K. Rausch [a,f], Inka Tertinegg [c], C. Ross Ethier [a,b,c,g,*]

[a] Mechanical and Industrial Engineering, University of Toronto, 5 King's College Rd., Toronto, Ontario M5S 3G8, Canada
[b] Institute of Biomaterials and Biomedical Engineering, University of Toronto, 164 College St., Room 407, Toronto, Ontario M5S 3G9, Canada
[c] Ophthalmology and Vision Sciences, University of Toronto, 399 Bathurst St., Room 7E-401 & 403, Toronto, Ontario M5T 2S8, Canada
[d] School of Optometry, University of Waterloo, 200 University Ave West, Waterloo, Ontario N2L 3G1, Canada
[e] Department of Biomedical Engineering, Tulane University, Lindy Boggs Center Suite 500, New Orleans, LA 70118, USA
[f] Institute for Computational Mechanics, Technische Universität München, Arcisstr. 21, Munich 80333, Germany
[g] Bioengineering, Imperial College London, South Kensington Campus, London SW7 2AZ, United Kingdom

ARTICLE INFO

Article history:
Received 26 May 2009
Accepted in revised form 21 September 2010
Available online xxx

Keywords:
sclera
glaucoma
biomechanics
optic nerve head
lamina cribrosa
intraocular pressure

ABSTRACT

Scleral thickness, especially near the optic nerve head (ONH), is a potential factor of interest in the development of glaucomatous optic neuropathy. Large differences in the dimensions of the sclera, the principal load-bearing tissue of the eye, have been observed between individuals. This study aimed to characterize the effects of these differences on ONH biomechanics. Eleven enucleated human globes (7 normal and 4 ostensibly glaucomatous) were imaged using high-field microMRI and segmented to produce 3-D individual-specific corneoscleral shells. An identical, idealized ONH geometry was inserted into each shell. Finite element modeling predicted the effects of pressurizing the eyes to an IOP of 30 mmHg, with the results used to characterize the effect of inter-individual differences in scleral dimensions on the biomechanics of the ONH. Measurements of the individual-specific corneoscleral shells were used to construct a 2-D axisymmetric idealized model of the corneoscleral shell and ONH. A sensitivity analysis based on this model quantified the relative importance of different geometrical characteristics of the scleral shell on the biomechanics of the ONH. Significant variations were observed in various measures of strain in the idealized lamina cribrosa (LC) across the seven normal corneoscleral shells, implying large differences in individual biomechanics due to scleral anatomy variations alone. The sensitivity analysis revealed that scleral thickness adjacent to the ONH was responsible for the vast majority of variation. Remarkably, varying peripapilary scleral thickness over the physiologically measured range changed the peak (95th percentile) first principal strain in the LC and radial displacement of the ONH canal by an amount that was equivalent to a change in IOP of 15 mmHg. Inter-individual variations in scleral thickness, particularly peripapillary scleral thickness, can result in vastly different biomechanical responses to IOP. These differences may be significant for understanding the interactions between IOP and scleral biomechanics in the pathogenesis of glaucomatous optic neuropathy. The relationship between scleral thickness and material properties needs to be studied in human eyes.

1. Introduction

Elevated intraocular pressure (IOP) is a well-accepted risk factor for the development of glaucomatous optic neuropathy. How IOP plays a role in the retinal ganglion cell loss characteristic of glaucoma is unclear; however, both IOP-dependent biomechanical and vascular effects have been suggested. The biomechanical model of the disease proposes that IOP-induced mechanical strain on the optic nerve head (ONH) leads to a cascade of events eventually culminating in retinal ganglion cell dysfunction and apoptosis (Burgoyne et al., 2005; Quigley et al., 1980). The mechanisms behind this cascade are not yet fully understood, although studies have identified the lamina cribrosa (LC) as an important site of damage (Quigley et al., 1980, 1981, 1983).

Although associated with elevated IOP, glaucoma is known to occur across the entire spectrum of IOP levels, suggesting the link

* Corresponding author at: Department of Bioengineering, Imperial College, Room B433, Level 4, Bessemer Building, South Kensington Campus, London SW7 2AZ, United Kingdom. Tel.: +44(0)20 7594 9795; fax: +44 (0)20 7594 9787.
E-mail address: r.ethier@imperial.ac.uk (C.R. Ethier).

0014-4835/$ – see front matter © 2010 Published by Elsevier Ltd.
doi:10.1016/j.exer.2010.09.014

between IOP and vision loss in glaucoma is complex (Sommer et al., 1991). It is possible that inter-individual differences in the biomechanics of the eye may play a role in determining the susceptibility to glaucomatous optic neuropathy. In particular, as the principal load-bearing tissue of the eye, the sclera likely plays a significant biomechanical role in the eye's response to IOP (Ethier, 2006). Previous work (Sigal et al., 2004, 2005, 2009a,b) shows that IOP-induced scleral deformations are transferred to the tissues of the ONH, including the LC. Significant differences in scleral thickness and geometry have been observed both by our group and others (Olsen et al., 1998; Norman et al., 2010), suggesting that there may also be wide variation in biomechanical behavior of the ONH. Furthermore, evidence of differences in scleral geometry in glaucomatous eyes, including thinning near the ONH, has been observed in both human (Ren et al., 2009; Norman et al., 2010) and monkey eyes (Downs et al., 2001). It therefore seems likely that it is important to consider these individual details when characterizing the biomechanics of the ONH.

Given the difficulty of directly measuring the biomechanics of the eye, most current work uses modeling. Some analytical modeling has been performed (Dongqi and Zeqin, 1999; Edwards and Good, 2001), but was subject to significant limitations due to the complexity of the geometry of the ONH. For this reason, researchers have adopted computational modeling using the finite element method, and much insight into the biomechanical behavior of the tissues of the ONH has been gained from successively more sophisticated models (e.g. Bellezza et al., 2000; Sigal et al., 2004, 2005).

Previous studies have shown that scleral material properties, geometry, and thickness have significant effects on the biomechanical environment of the ONH (Cahane and Bartov, 1992; Sigal et al., 2005). However, these studies both used uniform thickness spherical scleral shells, which is a significant simplification from physiological reality. Work with monkey eyes suggests a significant biomechanical role for the sclera (Girard et al., 2009a,b). Here our goal was to investigate the effects of physiologically realistic corneoscleral shell geometry on ONH biomechanics in human eyes. We did this by considering individual-specific and idealized "variable-geometry" corneoscleral shells based on MRI scans discussed previously (Norman et al., 2010). A "generic" optic nerve head (ONH) constructed using measurements from the literature (Sigal et al., 2004) was then placed into these shells, and the effects of different scleral shell anatomy on ONH biomechanics were computed. We find substantial biomechanical variations between individual eyes due to the sclera alone, and correlations between corneoscleral shell properties (specifically, scleral thickness, axial length, and shape) and the biomechanical environment in the ONH.

2. Materials and methods

The eyes were prepared, and the corneoscleral shell was imaged, segmented and measured using a technique described previously (Norman et al., 2010). Briefly, 11 enucleated human donor eyes were obtained from the Eye Bank of Canada within 24 h post-mortem. Seven of these eyes were identified as normal, while four were reported as glaucomatous by family members. The eyes were fixed with 10% formalin in phosphate buffered saline for 24 h at either 5 mmHg (right eyes; $n = 5$) or 50 mmHg (left eyes; $n = 6$). They were then scanned with a T1-weighted spin-echo 3-D protocol using a 7.0 T MRI scanner (Varian, Inc., Palo Alto, CA), providing 80 μm isotropic resolution over the whole eye. Amira 3.11 software (Mercury Computer Systems, Inc., Chelmsford, MA) was used to segment the MRI images, perform thickness measurements on the corneoscleral shell, and generate the 3-D meshes used in the measurement process. MATLAB (The Mathworks, Inc., Natick, MA) was used to post-process the thickness results. The eyes were oriented along an anterior-posterior axis running from the center of the ONH through the center of the cornea, and 15 equal radial length circumferential slices were made along this axis. Average scleral thickness was calculated for each circumferential slice, producing 15 measurements to characterize the thickness distribution of the corneoscleral shell.

2.1. Individual-specific models

This study aimed to determine the effects of physiologic variations in scleral geometry on the biomechanics of the ONH. In order to create a common basis for comparison between all models, an identical generic ONH geometry was chosen for all eyes. This had the advantage of separating the effects of the individual-specific corneoscleral shells from variations in ONH geometry and is a natural follow-up to previous work (Sigal et al., 2009a) identifying the sclera as a key biomechanical component in the eye's response to IOP. This previous study placed individual-specific ONHs into a generic scleral shell in order to understand the contribution of individual-specific ONH geometry to ocular biomechanics. The experiment described here examines the opposite scenario—individual-specific scleral geometry combined with a generic ONH—in order to isolate the effect of scleral geometry on ocular biomechanics. The generic ONH used in all corneoscleral shells was created from the geometry described in Sigal et al. (2004) and Sigal et al. (2005). It consisted of the peripapillary sclera, the LC, prelaminar neural tissue (the retina and choroid), postlaminar neural tissue (the optic nerve), and the pia mater, and was symmetrical about a central axis (axisymmetric).

The ostensibly glaucomatous shells, as discussed previously (Norman et al., 2010), were found to have smaller ONH canal radii and thinner posterior sclera than the normal eyes. The generic ONH geometry was found to be too big to fit in the ostensibly glaucomatous shells. For this reason, the glaucomatous shells were not included in the individual-specific analysis, although their dimensions were considered in an idealized analysis (discussed below).

In order to ensure a consistent ONH insertion into the sclera, the generic ONH was aligned into all seven shells using a MATLAB implementation of the iterative closest point (ICP) registration algorithm (Zhang, 1994). This algorithm minimizes the distance between two surfaces by minimizing an associated cost function. In this study, the cost was the sum of two components that measured the distances between the respective anterior scleral surfaces and ONH canal walls of the ONH and corneoscleral shell. Minimizing the former served to align the anterior scleral surface of the ONH with the interior scleral surface of the corneoscleral shell, whereas minimizing the latter helped to align the scleral canal in the ONH model with the scleral canal in the corneoscleral shell. A low-modulus interface material (see below) was inserted in areas where a stepped edge remained. In cases where the physiological scleral thickness exceeded that of the idealized sclera, all physiological sclera was conserved. Fig. 1 shows an example of a generic ONH inserted into an individual-specific corneoscleral shell.

The oriented ONHs were then combined with the individual-specific shells using voxel addition in Amira. The resulting surfaces were simplified to approximately 240,000 surface elements; when volume-meshed, this corresponded to approximately 1,000,000 10-noded tetrahedral finite elements. The geometry was exported into ANSYS 11.0 (ANSYS Inc., Canonsburg, PA), a commercial finite element analysis package, using a custom script. To provide additional geometrical detail in the ONH region, submodeling was performed. This involved creating a second, more-refined model of only the ONH and surrounding sclera for each eye. The boundary conditions and submodels were created using a methodology

Please cite this article in press as: Norman, R.E., et al., Finite element modeling of the human sclera: Influence on optic nerve head biomechanics and connections with glaucoma, Experimental Eye Research (2010), doi:10.1016/j.exer.2010.09.014

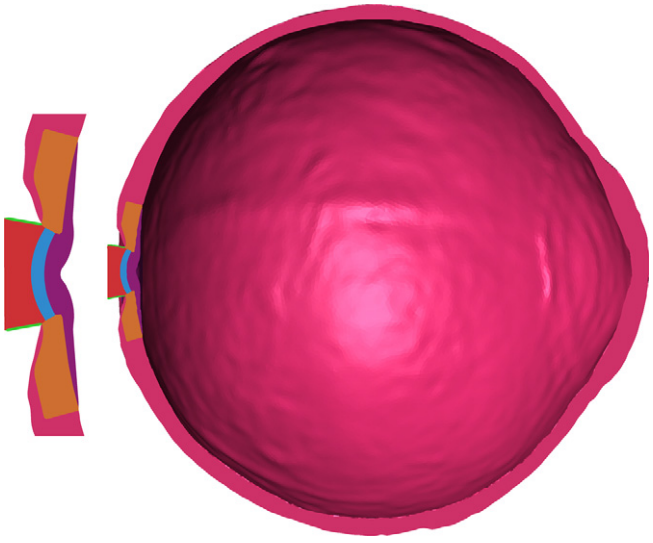

Fig. 1. Cross-sectional view of an individual-specific corneoscleral shell (pink) with an inserted generic ONH. Note the good central alignment of the ONH and the smooth interface with the interior surface of the sclera resulting from use of the iterative closest point registration algorithm. The retina (purple in this picture), would usually cover much of the interior of the eye; because of its mechanical weakness, however, it is unlikely to play a significant mechanical role relative to the sclera and so is only included in the region of interest, the ONH. The orange region denotes the inserted peripapillary scleral region. Blue represents the LC, red represents the optic nerve tissue, and green represents the pia mater. (For interpretation of the references to color in this figure legend, the reader is referred to the web version of this article.).

similar to the one described in (Beisheim and Sinclair, 2003) using tools in ANSYS. Numerical convergence was tested using a published technique (Beisheim and Sinclair, 2003). Calculated discretization and boundary condition error, two measures of convergence in submodeling, were both less than 1%.

Model parameters matched those used in a previous study (Sigal et al., 2004). Tissues were assumed to be linearly elastic, isotropic, and incompressible, although a Poisson ratio of 0.49 rather than 0.50 was selected to avoid non-convergent numerical behavior. This has previously been demonstrated to have little effect on results (Sigal et al., 2004). Tissue elastic moduli were based on those published in the literature: sclera 3 MPa, LC 0.3 MPa, pre- and post-laminar neural tissue 0.03 MPa, and pia mater 3 MPa. The interface material was assigned a modulus of 0.03 MPa. The eye models were pressurized to 30 mmHg from a resting pressure of 0 mmHg. Nodes at the apex of the cornea were constrained in all degrees of freedom, with the eye models otherwise free to inflate. Results were post-processed using ANSYS and Excel (Microsoft, Inc., Redmond, WA).

Mean and peak (95th percentile) 1st, 2nd, and 3rd principal strains in the LC were used as outcome measures. Strain represents the amount of stretch a tissue undergoes in response to a load. This deformation may be important in glaucomatous damage (Burgoyne et al., 2005; Sigal and Ethier, 2009). Defining a representative strain quantity can be complex due to the fact that strain is a tensor quantity, so that it cannot be specified completely by a single value at a given location. Typically, this is accounted for by using principal strains, a formulation where strain at a given location can be represented by three orthogonal values known as the 1st, 2nd, and 3rd principal strains. Physically, the first principal strain can be interpreted as the maximum tissue extension, while the third principal strain represents the maximum tissue compression (indicated by a negative sign (Sigal et al., 2007)). The reporting of strain is further complicated by the fact that, in general, a given strain measure will vary with position, so that for example, the LC experiences a distribution of strains over its volume. To account for this, we report the 95th percentile strain in the LC, i.e. the strain magnitude for which 95% of computed strain values in the lamina are smaller and 5% are greater. The top 5% of strain values were not considered as they could be the result of localized strain extrema caused by distortions in the finite element mesh, and hence might not be physically meaningful. The 95th percentile strain should therefore be considered as a measure of the peak strain experienced in the LC, which we assume represents the most potent mechanical stimulus experienced by the LC. The mean strain within the LC will be less than this 95th percentile peak value.

2.2. Idealized axisymmetric corneoscleral shell

Although physiologically accurate, the complex geometry of the individual-specific corneoscleral shell models made it difficult to identify which geometrical factors had the greatest influence on strains in the LC. Also, due to the variability in shell geometry, we decided to exclude the glaucomatous shells from the individual-specific analysis. To estimate the relative importance of different features of the geometry of the sclera and consider a broader range of scleral geometries, an axisymmetric scleral shell was constructed in ANSYS for use in a sensitivity analysis. An axisymmetric ONH geometry identical to the one used in the individual-specific corneoscleral shells was incorporated into this axisymmetric model. The models were meshed in a manner similar to one described previously (Sigal et al., 2004). Material properties matched those used in the individual-specific models.

The geometry of the axisymmetric shell was designed to allow independent adjustment of eye size, shape, and scleral thickness to facilitate modeling a wide range of eyes. Fig. 2 shows an example of the axisymmetric scleral model with all adjustable factors labeled. Table 1 lists the factors and their respective ranges. Each range was defined by the physiological range measured over the 11 human eyes included in this study. Thickness was specified using the circumferential average scleral thickness (i.e. the average across all four quadrants) measured for each slice in an earlier scleral thickness study (Norman et al., 2010).

As illustrated in Fig. 3 and described in detail below, the shell was composed of two regions: a truncated sphere forming the posterior sclera and a truncated ellipsoid forming the anterior sclera. Although a simpler spherical shell was originally tested (as had been used previously (Bellezza et al., 2000; Cahane and Bartov, 1992; Sigal et al., 2004)), it was found to match poorly with the shape of axially-elongated eyes, of which there were several in this study. Correctly representing axial elongation was judged to be important, since the companion paper and the literature (Ren et al., 2009) has observed that this feature is present in some glaucomatous eyes. Fig. 4 compares spherical and two region shells fitted to the dimensions of an actual axially-elongated eye.

The fitting procedure was as follows: the radius (termed "posterior radius" in Fig. 2) of the truncated sphere was determined by fitting a sphere to the posterior and posterior-equatorial scleral regions (Fig. 2). These regions were chosen since they gave the best approximation of the shape of the posterior sclera. Using smaller regions closer to the ONH for fitting tended to result in measurements that were influenced significantly by local geometry fluctuations. Using larger regions (e.g. the posterior hemisphere) in axially elongated eyes tended to result in a sphere that did not match the shape of the sclera close to the ONH. The actual fitting to the posterior and posterior-equatorial regions was done in MATLAB using a technique that minimized the distance between the sphere's surface and the scleral surface by varying the sphere's

Please cite this article in press as: Norman, R.E., et al., Finite element modeling of the human sclera: Influence on optic nerve head biomechanics and connections with glaucoma, Experimental Eye Research (2010), doi:10.1016/j.exer.2010.09.014

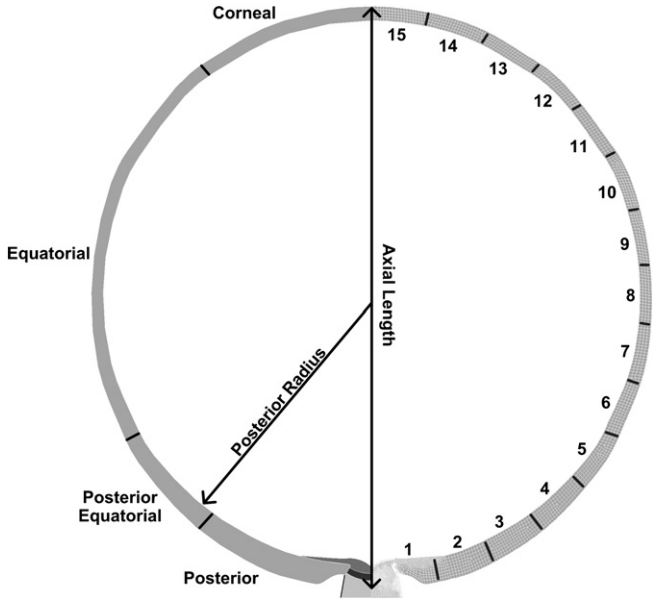

Fig. 2. The axisymmetric model with all geometric factors labeled. Each factor could be varied independently in the sensitivity study. The regions labeled at the left identify the simplified thickness distribution of the human eye observed in the companion paper. Models incorporating uniform thickness within some of these regions were used during the analysis. The numbers at the right correspond to the 15 regions where circumferential corneoscleral thickness measurements were made on each corneoscleral shell. Axial length was defined from the posterior aspect of the peripapillary sclera to the anterior of the cornea. Posterior radius defines a uniform spherical shape for the posterior region of the sclera (Fig. 3). It was measured on the individual-specific corneoscleral shells by fitting a sphere to the interior surface of the sclera of the posterior-equatorial and posterior regions (darkened), as described in more detail in the text. An idealized ONH with identical geometry (pictured at bottom) was included in all shell models.

location and radius. After the truncated sphere was defined, the truncated ellipsoid was determined as follows: the truncated sphere and the truncated ellipsoid were forced to meet at the equator and their slopes were forced to match at the junction, so that the scleral surface was smooth and free of non-physiological sharp intersections that might affect the biomechanics. Finally, the truncated ellipsoid was chosen so that the model had the correct axial length of the eye.

Shell thickness was independently adjustable in each of the 15 regions described in our previous study of scleral thickness (Fig. 2; Norman et al., 2010). Splines were fit between adjacent regions to ensure a smooth transition between regions of different thickness; at the intersections of two splines, the slopes of the end segments were set equal to one another.

Although idealized, the axisymmetric models should be biomechanically representative of the physiological individual-specific shells. To confirm this, an axisymmetric model was created from each individual-specific shell, and the axisymmetric model and its corresponding individual-specific shell were biomechanically analyzed in ANSYS. Comparing mean 1st, 2nd, and 3rd principal strains in the LC between corresponding models indicates that the axisymmetric models served as reasonable estimators of LC strain in the individual-specific models despite being greatly simplified: the average relative difference in percent strain calculated was ±8.0% (e.g. if 5% strain was calculated in the LC of the 2D model, then a strain of between 4.6 and 5.4% would be expected in the 3D model). Similar tests with spherical axisymmetric shells showed greater errors, supporting the decision to use a two region model. Furthermore, the two region model allowed independent variation of axial length and shape at the posterior of the eye during the sensitivity analysis.

Table 1
Factors and ranges used in sensitivity analysis.

All measurements expressed in μm		
Factor	Minimum	Maximum
Slice 1 thickness	720	1326
Slice 2 thickness	676	1228
Slice 3 thickness	692	1174
Slice 4 thickness	661	1081
Slice 5 thickness	528	892
Slice 6 thickness	435	735
Slice 7 thickness	386	679
Slice 8 thickness	373	633
Slice 9 thickness	417	630
Slice 10 thickness	471	658
Slice 11 thickness	450	629
Slice 12 thickness	462	693
Posterior polar thickness[a]	691	1222
Posterior equatorial thickness	588	977
Equatorial thickness	432	631
Corneal thickness[b]	551	551
Axial length[c]	23,793	28,536
Posterior eye radius	10,858	12,705

[a] Four distinct thickness regions of the eye were observed in the companion study. Briefly, the posterior polar, posterior equatorial, equatorial, and corneal regions correspond to slices 1–3, 4–5, 6–12, and 13–15 of the 15 equal radial length slices made in the eye. In terms of axial length of the eye, the regions correspond to 0–10%, 10–25%, 25–90%, and 90–100% of the axial length of the eye measured from the ONH to the cornea.

[b] Post-mortem corneal swelling is a known phenomenon. For this reason, our own corneal thickness measurements were not included. Instead, an average corneal thickness was assumed for all eyes based on data in the literature (Wolfs et al., 1997; Yaylali et al., 1997). It is unclear whether sclera is subject to a similar effect (Olsen et al., 1998). Unlike the corneal thickness, however, scleral thickness is not dependent on active transport processes, so there is little reason to believe it will change post-mortem.

[c] Axial length was measured from the most posterior aspect of the ONH sclera to the most anterior aspect of the cornea as described in our previous study of scleral thickness (Norman et al., 2010).

2.3. Sensitivity analysis

We conducted a sensitivity analysis to characterize the effect of each geometric factor (e.g. peripapillary scleral thickness) on a given response variable (e.g. 95th percentile 1st principal strain in the LC). Because we could vary each factor in the axisymmetric shell independently, the effects were clearer than in the individual-

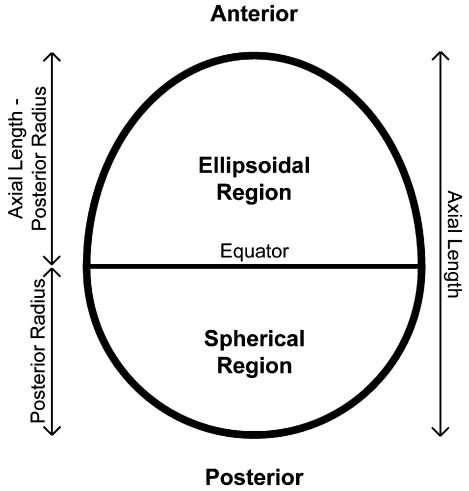

Fig. 3. The axisymmetric corneoscleral shell model consisted of two regions: an anterior truncated ellipsoid and a posterior truncated sphere, as described in detail in the text. This provided a more physiological eye shape in the case of axially-elongated eyes and allowed independent variation of the shape of the posterior region of the eye and axial length of the eye.

Please cite this article in press as: Norman, R.E., et al., Finite element modeling of the human sclera: Influence on optic nerve head biomechanics and connections with glaucoma, Experimental Eye Research (2010), doi:10.1016/j.exer.2010.09.014

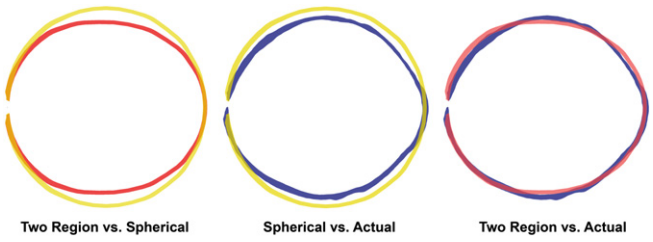

Fig. 4. Comparison of a spherical shell (yellow) versus a two region shell (red), both of which were fitted to match the dimensions of an actual eye (blue). Colors have been made transparent to facilitate comparison. The two axisymmetric shells are compared on the left. The center and right panels compare the axisymmetric shells against the actual eye. The two region model provided a more physiologically accurate shape in the case of an axially-elongated eye, especially in matching the shape of the posterior sclera. When fit to a non-axially-elongated eye, the two region model became spherical (e.g. as in Fig. 2) (For interpretation of the references to color in this figure legend, the reader is referred to the web version of this article.).

specific models, where the effects of all factors are confounded. The sensitivity analysis was performed using a 2^k factorial design technique (one variant of the Design of Experiments method) in ANSYS (Allen, 2006; Montgomery et al., 2004). This approach has been shown to be superior to a conventional sensitivity analysis (where each factor is varied individually with the others held constant), since it varies all factors simultaneously; through this approach, factor interactions, where, for example, the effects of two factors varied together is different from their individual effects, can then be accounted for (Sigal, 2009). It also allows a quantitative determination of the relative strength of different factors in terms of their effects on a response variable. Briefly, a factorial design evaluates models at the maximum and minimum value of each factor and observes the effect on a chosen response variable. This leads to 2^k experiments (where k is the number of factors), corresponding to all possible combinations of conditions.

The effect of a factor on a response variable was determined by calculating the main effect and two and three factor interactions. Briefly (see Montgomery et al., 2004; Allen, 2006 for details), the main effect is an aggregate measure that estimates the overall impact on the response variable by comparing all of the models where a factor is at its maximum to all of the models where it is at its minimum. It is expressed in the units of the response variable (so, if modeling the effect of a factor on displacement in μm, the main effect will be expressed in μm), and estimates the average effect of varying the factor over the specified range. Two and three factor interactions measure the effects of all pairings (e.g. axial length and slice 1 thickness) and triplings (e.g. axial length, slice 1 thickness, and equatorial thickness) on the response variable. Calculating an interaction involves comparing cases where all factors are assigned to the same value (i.e. their respective maximums or minimums) versus cases where their values differ (e.g. one factor at maximum and another factor at minimum in the case of a pair). Interactions are also expressed in the units of the response variable. They can be informative as they can identify cases where the behavior of the response variable is different from what would be expected by the main effect of a factor.

In the factorial design used in this study, seven factors were varied: thicknesses in scleral slices 1 through 3, thickness of the posterior-equatorial scleral region, thickness of the equatorial scleral region, axial eye length, and posterior eye radius. The thickness of the corneal region was held constant at 551 μm, an average value taken from the literature (Wolfs et al., 1997; Yaylali et al., 1997). The choice of factors was motivated in part by linear discriminant analysis of the results of the individual-specific eyes (Norman, 2008). The posterior region of the sclera was split into its component slices (slices 1–3) to provide additional detail in the proximity of the ONH as preliminary studies showed that this region was responsible for the vast majority of variation in LC strain level. The range of each factor was defined by the physiological range measured across the 11 eyes (Table 1).

Two output measures, peak (95th percentile) 1st principal strain in the LC and radial displacement of the ONH canal, were used as the response variables in the factorial analysis. Both were chosen based on interpretation of the physiology of the ONH. The 95th percentile 1st principal strain in the LC is indicative of the maximum extension in the LC, and hence can be used as an estimate of sclera-induced LC deformation. The 95th percentile value was chosen over the maximum strain in order to avoid artifactual results from issues such as malformed elements in the finite element mesh. Radial displacement of the ONH canal was measured at the location on the sclera contacting the furthest radial extent of the posterior aspect of the LC, and hence is also indicative of LC deformation. It also may provide insight into how scleral deformation can affect the biomechanical environment of the LC. Finally, mean strains were collected to measure the average stretch in the lamina cribrosa; also, comparison of mean and 95th percentile strains gives some indication about the variation in strain globally across the LC.

3. Results

3.1. Individual-specific models

Large variations in LC strain were observed between different corneoscleral shells (Fig. 5): mean first, second, and third principal strains measured 2.1% to 3.1%, 1.3% to 2.2%, and −3.4% to −5.1%, respectively, over the 11 eyes; 95th percentile first, second, and third principal strain measured 2.4% to 4.6%, 1.6% to 3.2%, and −3.8% to −7.3%, respectively. This suggests that geometry differences between corneoscleral shells can have significant biomechanical consequences for ONH tissues.

3.2. Sensitivity analysis using idealized axisymmetric corneoscleral shell

Significant variations in LC strains and scleral canal radial displacement were observed over the physiological range of factors included in the factorial design: 95th percentile first principal strain

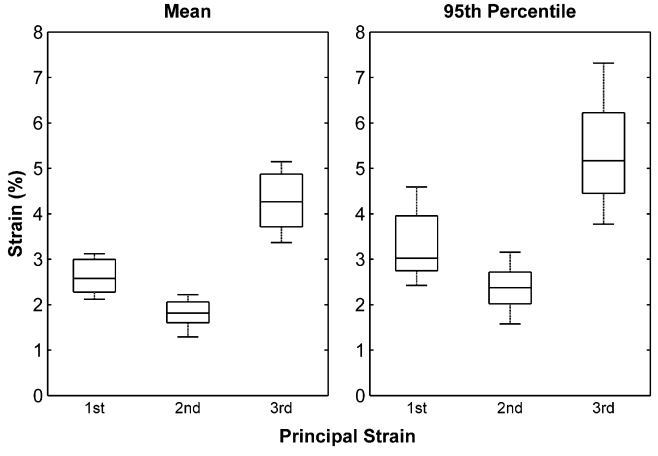

Fig. 5. Box and whisker plots of mean and 95th percentile strains observed in the lamina cribrosa of seven individual-specific corneoscleral shell models. The bottom and top of the boxes represent the 25th and 75th percentiles while the center line represents the median. The whiskers extend to the most extreme data points. See text for the interpretation of the first, second and third principal strains. The sign of the third principal strain has been reversed to facilitate plotting.

Please cite this article in press as: Norman, R.E., et al., Finite element modeling of the human sclera: Influence on optic nerve head biomechanics and connections with glaucoma, Experimental Eye Research (2010), doi:10.1016/j.exer.2010.09.014

in the LC varied from 1.9% to 5.2% and ONH canal radial displacement varied from 16 μm to 40 μm over the 128 models. Mean strain across the whole LC varied between 1.8% and 3.6% over the models. Fig. 6 shows the main effects and significant interactions calculated in the study. It is clear that the relative importance of each factor was strongly correlated between the two measures (95th percentile first principal strain in the LC and ONH canal radial displacement), suggesting consistent effects on ONH biomechanics. The two factor and three factor interactions not shown on the plot were all at least an order of magnitude lower than the main effects and so were considered negligible.

The sensitivity analysis showed that slice 1 thickness, i.e. the thickness of the peripapillary sclera, played by far the most significant role in the biomechanical response of the ONH: the magnitude of its main effect was 70% of the entire range of strain and displacement seen across all models. The posterior radius had a smaller but still significant effect, suggesting that the shape of the posterior of the eye can alter its biomechanical response. The positive correlation of increased posterior radius with increased strain and displacement suggests that a flatter posterior sclera (i.e. one with lower curvature) may lead to higher biomechanical loads in the ONH.

Increasing the thickness of slices 2 and 3 slightly increased strain and displacement in the LC rather than decreasing it, contrary to the effect of slice 1 thickness. Examination of modeling results showed that this was due to a change in the geometry of the loading of the ONH (Fig. 7), which may be indicative of a peculiarity of the model geometry, but could also represent more complex mechanical interactions between the tissues of the eye. It is possible that particular scleral geometries may transfer their IOP-induced deformations more effectively to the LC than others. The interactions observed in the factorial design support the idea that the interplay of different geometrical characteristics can lead to more complex effects.

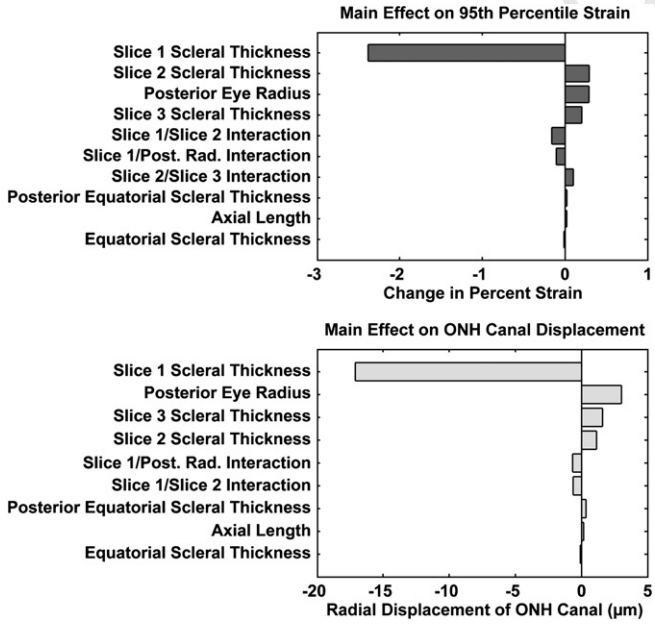

Fig. 6. Main effects of input factors on two response measures: 95th percentile first principal strain in the lamina cribrosa (top panel) and ONH canal radial displacement (bottom panel). The length of the bars describes the strength of the input factors (listed on the left of the bar) calculated in the factorial analysis. The signs indicate the nature of the relationship between the factor and the response variable, with a negative sign denoting an inverse relationship. For example, varying slice 1 scleral thickness from the minimum to maximum value observed in this study can be expected to cause an average decrease in 95th percentile 1st first principal percent strain of 2.4% (e.g. from 5.2% to 2.8%) at 30 mmHg. The effects of posterior-equatorial thickness, equatorial thickness, and axial length were negligible.

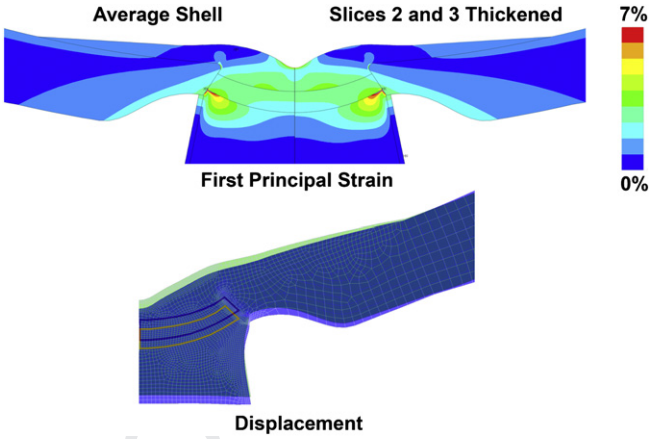

Fig. 7. Plots comparing the strain and displacement of an idealized ONH for a corneoscleral shell of average dimensions versus a corneoscleral shell with slices 2 and 3 at their maximum values. The LC has been outlined in black. Small differences are visible in the strain contour plots, including a larger high-strain region at the perimeter. Note that despite its small size on a 2-D plot, this region comprises a large volume in three dimensions. Differences are also evident between the average (green with black lamina cribrosa outline) and the thickened (transparent blue with orange LC outline) models in the displacement plot. The overlapping region between the two models is dark blue. The thickened shell displaces further in the posterior direction than the average shell, resulting in changes in the geometry of the scleral canal. These changes are the likely source of the increased strain evident in the contour plots. Displacements on the lower plot were scaled to better highlight differences between the models.

Given the dominant effect of slice 1 scleral thickness on the biomechanics of the ONH, an investigation was performed to observe its importance relative to changes in IOP. Ten models with slice 1 thicknesses spaced evenly across the physiological range observed over the 11 eyes (720 μm to 1326 μm) were elevated from 0 mmHg to normal (15 mmHg) and significantly elevated (30 mmHg) IOP levels. Axial length, posterior radius, and the other regional thicknesses were all set to average values.

The results showed that varying slice 1 thickness over the physiological range resulted in a change in 95th percentile 1st principal LC strain and radial ONH canal displacement equivalent to a 15 mmHg change in IOP (Fig. 8). This suggests that eyes with thinned peripapillary sclera—as may be the case in glaucomatous eyes—may be vastly more sensitive to IOP than eyes with thicker sclera.

4. Discussion

The goal of this study was to characterize the effect of scleral shell anatomy (geometry) on ONH biomechanics, and to specifically identify which geometrical features of the sclera were most influential in ONH biomechanics. This information is valuable for developing more physiologically accurate ocular biomechanical models and may provide insight into the relationship between IOP and the development of glaucomatous optic neuropathy.

A major result of this work was the observation of a large variation in ONH biomechanical response across different eyes: 95th percentile first principal strain in the LC, ONH radial canal displacement, and mean strain across the LC all varied by more than a factor of two across the range of models in the sensitivity analysis. This is strong evidence that the anatomy of the sclera can have significant effects on the biomechanics of the ONH. One implication is that future ocular biomechanical models of the ONH should incorporate a physiologically-representative sclera. The results of

Please cite this article in press as: Norman, R.E., et al., Finite element modeling of the human sclera: Influence on optic nerve head biomechanics and connections with glaucoma, Experimental Eye Research (2010), doi:10.1016/j.exer.2010.09.014

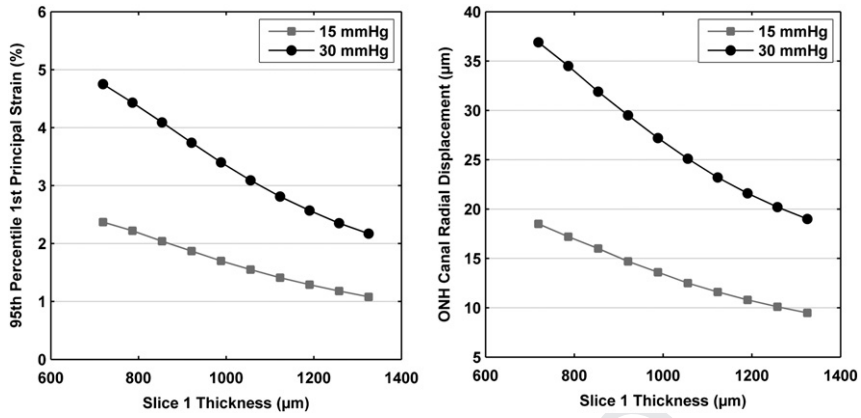

Fig. 8. Effect of varying slice 1 thickness on 95th percentile 1st principal strain in the lamina cribrosa (left panel) and ONH canal radial displacement (right panel) for two IOP levels. For example, a model with slice 1 thickness of 1326 μm pressurized to 30 mmHg has similar strain and displacements to those observed in a model with slice 1 thickness of 720 μm at 15 mmHg. Also, it can be seen that strain and displacement both approximately double between the thickest and thinnest sclera models at both IOP levels, suggesting potentially large inter-individual differences in ONH biomechanics.

the sensitivity analysis suggest that matching the characteristics of the peripapillary sclera is most important.

More generally, this observation confirms that there may be significant inter-individual differences in biomechanical behavior stemming from differences in the anatomy of the sclera. The individual-specific models support this strongly: strain level varied across the eyes by between 47 and 100 percent, depending on the strain quantity measured. Perhaps even more significant is the fact that this variation was observed over only seven eyes—larger differences in anatomy likely exist across the entire population. Furthermore, the range of LC strain observed in both studies reach the threshold of what may be biologically significant: in vitro studies of neuronal cells found a wide range of biological effects at strains of 5–6% (Edwards and Good, 2001; Margulies and Thibault, 1992).

The sensitivity analysis helped identify what geometrical traits of the eye would result in the greatest sensitivity to IOP. We found that the thickness of the posterior sclera—and particularly that of the peripapillary sclera defined by slice 1—had a strong effect on the biomechanics of the ONH. This is of particular interest in light of previous observations of scleral thinning in glaucoma. The source of this thinning is unclear, but there is some evidence that it is the result of scleral remodeling, perhaps in response to IOP. Studies in the literature have linked posterior scleral thinning in both humans and monkeys with elevated IOP (Downs et al., 2001; Tane and Kohno, 1986). If this is the case, it could have a significant effect on the biomechanical response of the ONH to IOP.

The potential importance of this is illustrated by our modeling of the effect of varying slice 1 (peripapillary) scleral thickness versus IOP level. The results show that varying peripapillary scleral thickness alone over the observed physiological range is equivalent to a significant change in IOP level. Considering the likelihood that other significant factors such as the geometry and material properties of the ONH also vary between individuals, structural differences between eyes could lead to vastly different sensitivity to IOP. The large variation in strain level seen in the individual-specific models supports this hypothesis. These observations could also explain IOP's complex relationship with the development of glaucoma.

This study is subject to several limitations. The most important limitation is that our study only examined the effects of scleral thickness on ONH biomechanics and did not investigate differences in scleral material properties, which have previously been demonstrated to have a strong effect on ONH biomechanics (Sigal et al., 2005; Sigal, 2009). It is possible that there is a compensatory mechanism whereby individuals with thinner sclera have tissue that is stiffer, resulting in similar biomechanical behavior to a thicker, weaker tissue. Reported material properties for human sclera vary widely (Sigal et al., 2004), suggesting that there could be significant inter-individual differences. Although technically challenging, it therefore seems very important to examine how stiffness and thickness co-vary in the sclera, although preliminary data (Eilaghi et al., 2009) suggest that the co-variance may be small.

Assuming linear material properties for the tissues of the ONH is a simplification. However, there is still surprisingly little information on the nonlinear properties of ONH tissues. To the best of our knowledge there is no published data on the nonlinear properties of the LC, the prelaminar or retrolaminar tissues, or the pia mater. There are, however, some recent reports on the nonlinear properties of the sclera (Girard et al., 2009a,b; Spoerl et al., 2005), although these data were collected either in monkey eyes or at high strain. Work is currently underway to incorporate nonlinear material properties into future models. Our selection of material properties is consistent with recently published models of the posterior pole, such as those of Roberts and Downs (Downs et al., 2009; Roberts et al., 2010) and Sigal (Sigal et al., 2009a,b; Sigal, 2009). Also, although tissues are usually thought of as viscoelastic, the slow development of glaucomatous damage, which typically occurs over months or years, means that assuming elastic behavior is reasonable.

Also to be considered when interpreting the results is our choice of outcome measures. Although these were chosen based on our best understanding of the physiology of the ONH, they are ultimately arbitrary. However, the outcome measures we chose are certainly indicative of biomechanical differences between eyes, whether or not they directly represent the mechanical effects that may play a role in the pathophysiology of glaucoma, and have been used in several previous biomechanical studies of the ONH (Edwards and Good, 2001; Roberts et al., 2010; Sander et al., 2006; Sigal et al., 2005; Sigal et al., 2009a,b).

Many of the parameters used in this study were idealized. All models used an identical idealized ONH in order to facilitate comparisons. Because of this, any differences in the ONH region, which could likely lead to significant variability in results, are not accounted for. Furthermore, all models employed highly idealized material properties, which likely have a great effect on the outcome measures. Although it would be interesting to include more realistic material properties, precious few are currently readily

Please cite this article in press as: Norman, R.E., et al., Finite element modeling of the human sclera: Influence on optic nerve head biomechanics and connections with glaucoma, Experimental Eye Research (2010), doi:10.1016/j.exer.2010.09.014

available. Despite these downsides, however, these simplifications also confer some benefits: idealizations make it easier to identify and interpret some effects and, in our case, enable straightforward comparisons.

Although more robust than a conventional sensitivity analysis, factorial design still has limitations. The main effects calculated are dependent on the range specified for a given factor, meaning that a larger range may result in a greater main effect. This potential pitfall, however, has applied to all published sensitivity analyses (Sigal et al., 2004, 2005, 2009a,b). This work, however, improves upon these by using ranges determined from direct measurements of human eyes, meaning that they are representative of the actual physiological range.

Our use of an axisymmetric model in the sensitivity analysis means that we are unable to comment on the potentially interesting effects of differences in scleral thickness between quadrants. An axisymmetric model was chosen to simplify interpretation of the data. Furthermore, for this analysis we assumed that factors varied independently of each other (e.g. thickness at the pole was not associated with thickness at the equator), which may not be the case in vivo. We varied the factors independently for two reasons: first, because factor covariations are unknown; second, because this allowed us to determine factor influences both independently and in interaction. From the factor influences identified from independent variations it would be relatively straightforward to determine the factor combined effects if and when factor covariations are measured experimentally.

The 3-D physiological shells used in this work were pressurized to 5 mmHg or 30 mmHg as previously described. A non-zero pressure was necessary in order to avoid artefactual effects such as folding of the tissue during imaging. In all modeling, however, the initial pressure was assumed to be zero. Although reasonable in the case of the eyes fixed at 5 mmHg, this appears counterintuitive for the eyes fixed at 50 mmHg. Previous simulations and experimental studies in both human (Sigal et al., 2010) and monkey (Roberts et al., 2010; Yang et al., 2009) have reported that IOP-related deformations are small compared with inter-individual variations, however. This is consistent with our observation of no statistically significant differences in scleral geometry at the different fixation pressures (Norman et al., 2010), although this may be due to limitations of our imaging resolution. Hence we believe that it was reasonable to assume all models to be at the same initial (zero) pressure.

In summary, we have modeled the biomechanics of both individual-specific corneoscleral shells and idealized axisymmetric corneoscleral shells in order to better understand the effect of inter-individual differences in scleral anatomy on the biomechanics of the ONH. At a constant IOP level, we found large variations in both strain in the LC and ONH canal displacement across the different models, confirming that the sclera plays a significant biomechanical role. Sensitivity analysis revealed that the vast majority of these variations were caused by the sclera directly adjacent to the ONH (peripapillary sclera) and that the thickness of this region had a strong effect on ONH biomechanics. Pairing this observation with evidence that this region may thin in glaucoma suggests that the sclera may play a significant biomechanical role in the disease. Further investigation of the thickness and material properties of this region in normal and glaucomatous eyes may be informative.

Acknowledgements

The authors thank the Eye Bank of Canada for providing donor tissue. The authors also thank the Mouse Imaging Centre for their help in preparing and imaging the eyes.

References

Allen, T.T., 2006. Introduction to Engineering Statistics and Six Sigma. Springer-Verlag, London.
Beisheim, J.R., Sinclair, G.B., 2003. On the three-dimensional finite element analysis of dovetail attachments. ASME J. Turbomach. 125, 372–379.
Bellezza, A.J., Hart, R.T., Burgoyne, C.F., 2000. The optic nerve head as a biomechanical structure: initial finite element modeling. Invest. Ophthalmol. Vis. Sci. 41, 2991–3000.
Burgoyne, C.F., Downs, J.C., Bellezza, A.J., Suh, J.K., Hart, R.T., 2005. The optic nerve head as a biomechanical structure: a new paradigm for understanding the role of IOP-related stress and strain in the pathophysiology of glaucomatous optic nerve head damage. Prog. Retin. Eye Res. 24, 39–73.
Cahane, M., Bartov, E., 1992. Axial length and scleral thickness effect on susceptibility to glaucomatous damage: a theoretical model implementing Laplace's law. Ophthalmic Res. 24, 280–284.
Dongqi, H., Zeqin, R., 1999. A biomathematical model for pressure-dependent lamina cribrosa behavior. J. Biomech. 32, 579–584.
Downs, J.C., Ensor, M.E., Bellezza, A.J., Thompson, H.W., Hart, R.T., Burgoyne, C.F., 2001. Posterior scleral thickness in perfusion-fixed normal and early-glaucoma monkey eyes. Invest. Ophthalmol. Vis. Sci. 42, 3202–3208.
Downs, J.C., Roberts, M.D., Burgoyne, C.F., Hart, R.T., 2009. Multiscale finite element modeling of the lamina cribrosa microarchitecture in the eye. Conf. Proc. IEEE Eng. Med. Biol. Soc. 2009, 4277–4280.
Edwards, M.E., Good, T.A., 2001. Use of a mathematical model to estimate stress and strain during elevated pressure induced lamina cribrosa deformation. Curr. Eye Res. 23, 215–225.
Eilaghi, A., Flanagan, J.G., Tertinegg, I., Simmons, C.A., Brodland, G.W., Ethier, C.R., 2009. Biaxial mechanical evaluation of human sclera. Invest. Ophthalmol. Vis. Sci. 50, 4903.
Ethier, C.R., 2006. Scleral biomechanics and glaucoma–a connection? Can. J. Ophthalmol. 41, 9–12. 14.
Girard, M.J., Downs, J.C., Bottlang, M., Burgoyne, C.F., Suh, J.K., 2009a. Peripapillary and posterior scleral mechanics-Part II: experimental and inverse finite element characterization. J. Biomech. Eng. 131 051012.
Girard, M.J., Downs, J.C., Burgoyne, C.F., Suh, J.K., 2009b. Peripapillary and posterior scleral mechanics-part I: development of an anisotropic hyperelastic constitutive model. J. Biomech. Eng. 131 051011.
Margulies, S.S., Thibault, L.E., 1992. A proposed tolerance criterion for diffuse axonal injury in man. J. Biomech. 25, 917–923.
Montgomery, D.C., Runger, G.C., Hubele, N.F., 2004. Engineering Statistics, third ed. John Wiley & Sons, New York.
Norman R.E., 2008. Influence of the Scleral Shell on the Biomechanical Environment of the Human Optic Nerve Head. MASc Thesis, Department of Mechanical and Industrial Engineering, University of Toronto. 2008.
Norman, R.E., Flanagan, J.G., Rausch, S.M., Sigal, I.A., Tertinegg, I., Eilaghi, A., Portnoy, S., Sled, J.G., Ethier, C.R., 2010. Dimensions of the human sclera: thickness measurement and regional changes with axial length. Exp. Eye Res. 90, 277–284.
Olsen, T.W., Aaberg, S.Y., Geroski, D.H., Edelhauser, H.F., 1998. Human sclera: thickness and surface area. Am. J. Ophthalmol. 125, 237–241.
Quigley, H.A., Addicks, E.M., Green, W.R., Maumenee, A.E., 1981. Optic nerve damage in human glaucoma. II. The site of injury and susceptibility to damage. Arch. Ophthalmol. 99, 635–649.
Quigley, H.A., Flower, R.W., Addicks, E.M., McLeod, D.S., 1980. The mechanism of optic nerve damage in experimental acute intraocular pressure elevation. Invest. Ophthalmol. Vis. Sci. 19, 505–517.
Quigley, H.A., Hohman, R.M., Addicks, E.M., Massof, R.W., Green, W.R., 1983. Morphologic changes in the lamina cribrosa correlated with neural loss in open-angle glaucoma. Am. J. Ophthalmol. 95, 673–691.
Ren, R., Wang, N., Li, B., Li, L., Gao, F., Xu, X., Jonas, J.B., 2009. Lamina cribrosa and peripapillary sclera histomorphometry in normal and advanced glaucomatous Chinese eyes with various axial length. Invest. Ophthalmol. Vis. Sci. 50, 2175–2184.
Roberts, M.D., Liang, Y., Sigal, I.A., Grimm, J., Reynaud, J., Bellezza, A., Burgoyne, C.F., Downs, J.C., 2010. Correlation between local stress and strain and lamina cribrosa connective tissue volume fraction in normal monkey eyes. Invest. Ophthalmol. Vis. Sci. 51, 295–307.
Sander, E.A., Downs, J.C., Hart, R.T., Burgoyne, C.F., Nauman, E.A., 2006. A cellular solid model of the lamina cribrosa: mechanical dependence on morphology. J. Biomech. Eng. 128, 879–889.
Sigal, I.A., Flanagan, J.G., Tertinegg, I., Ethier, C.R., 2010. 3D morphometry of the human optic nerve head. Exp. Eye Res. 90, 70–80.
Sigal, I.A., 2009. Interactions between geometry and mechanical properties on the optic nerve head. Invest. Ophthalmol. Vis. Sci. 50, 2785–2795.
Sigal, I.A., Ethier, C.R., 2009. Biomechanics of the optic nerve head. Exp. Eye Res. 88, 799–807.
Sigal, I.A., Flanagan, J.G., Ethier, C.R., 2005. Factors influencing optic nerve head biomechanics. Invest. Ophthalmol. Vis. Sci. 46, 4189–4199.
Sigal, I.A., Flanagan, J.G., Tertinegg, I., Ethier, C.R., 2004. Finite element modeling of optic nerve head biomechanics. Invest. Ophthalmol. Vis. Sci. 45, 4378–4387.
Sigal, I.A., Flanagan, J.G., Tertinegg, I., Ethier, C.R., 2007. Predicted extension, compression and shearing of optic nerve head tissues. Exp. Eye Res. 85, 312–322.
Sigal, I.A., Flanagan, J.G., Tertinegg, I., Ethier, C.R., 2009a. Modeling individual-specific human optic nerve head biomechanics. Part I: IOP-induced deformations and influence of geometry. Biomech. Model. Mechanobiol. 8, 85–98.

Please cite this article in press as: Norman, R.E., et al., Finite element modeling of the human sclera: Influence on optic nerve head biomechanics and connections with glaucoma, Experimental Eye Research (2010), doi:10.1016/j.exer.2010.09.014

Sigal, I.A., Flanagan, J.G., Tertinegg, I., Ethier, C.R., 2009b. Modeling individual-specific human optic nerve head biomechanics. Part II: influence of material properties. Biomech. Model. Mechanobiol. 8, 99–109.

Sommer, A., Tielsch, J.M., Katz, J., Quigley, H.A., Gottsch, J.D., Javitt, J., Singh, K., 1991. Relationship between intraocular pressure and primary open angle glaucoma among white and black Americans. The Baltimore Eye Survey. Arch. Ophthalmol. 109, 1090–1095.

Spoerl, E., Boehm, A.G., Pillunat, L.E., 2005. The influence of various substances on the biomechanical behavior of lamina cribrosa and peripapillary sclera. Invest. Ophthalmol. Vis. Sci. 46, 1286–1290.

Tane, S., Kohno, J., 1986. The microscopic biometry of the thickness of the human retina, choroid and sclera by ultrasound. In: Proceedings of the XXVth International Congress of Ophthalmology, pp. 275–277.

Wolfs, R.C., Klaver, C.C., Vingerling, J.R., Grobbee, D.E., Hofman, A., de Jong, P.T., 1997. Distribution of central corneal thickness and its association with intraocular pressure: the Rotterdam Study. Am. J. Ophthalmol. 123, 767–772.

Yang, H., Downs, J.C., Sigal, I.A., Roberts, M.D., Thompson, H., Burgoyne, C.F., 2009. Deformation of the normal monkey optic nerve head connective tissue after acute IOP elevation within 3-D histomorphometric reconstructions. Invest. Ophthalmol. Vis. Sci. 50, 5785–5799.

Yaylali, V., Kaufman, S.C., Thompson, H.W., 1997. Corneal thickness measurements with the Orbscan Topography System and ultrasonic pachymetry. J. Cataract Refract. Surg. 23, 1345–1350.

Zhang, Z., 1994. Iterative point matching for registration of free-form curves and surfaces. Int. J. Comp. Vision 13, 119–152.

Please cite this article in press as: Norman, R.E., et al., Finite element modeling of the human sclera: Influence on optic nerve head biomechanics and connections with glaucoma, Experimental Eye Research (2010), doi:10.1016/j.exer.2010.09.014